JACS
JOURNAL OF THE AMERICAN CHEMICAL SOCIETY
Article
pubs.acs.org/JACS

Dynamics of Solvent-Mediated Electron Localization in Electronically Excited Hexacyanoferrate(III)

Wenkai Zhang,[§] Minbiao Ji, Zheng Sun, and Kelly J. Gaffney*

PULSE Institute, SLAC National Accelerator Laboratory, Stanford University, Menlo Park, California 94025, United States

Supporting Information

ABSTRACT: We have used polarization-resolved UV pump–mid-IR probe spectroscopy to investigate the dynamics of electron hole localization for excited-state ligand-to-metal charge-transfer (LMCT) excitation in $Fe(CN)_6^{3-}$. The initially generated LMCT excited state has a single CN-stretch absorption band with no anisotropy. This provides strong evidence that this initial excited state preserves the octahedral symmetry of the electronic ground state by delocalizing the ligand hole in the LMCT excited state on all six cyanide ligands. This delocalized LMCT excited state decays to a second excited state with two CN-stretch absorption bands. We attribute both peaks to a single excited state because the formation time for both peaks matches the decay time for the delocalized LMCT excited state. The presence of two CN-stretch absorption bands demonstrates that this secondary excited state has lower symmetry. This observation, in conjunction with the solvent-dependent time constant for the formation of the secondary excited state, leads us to conclude that the secondary excited state corresponds to a LMCT state with a localized ligand hole.

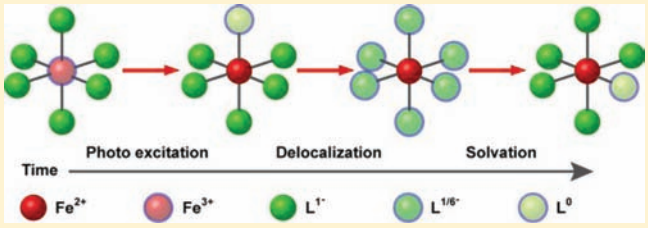

INTRODUCTION

Fast and efficient energy migration and charge separation represent essential steps in molecularly based light-harvesting materials, be they natural[1−6] or synthetic.[7−13] High symmetry and strong intermolecular coupling facilitate fast energy migration, while environmental disorder and solvation, as well as intramolecular distortion, lead to the symmetry breaking that facilitates charge separation. The interplay of electronic coupling and disorder, both dynamic and static, has a critical impact on the electron mobility in molecular materials[14−17] and the performance of light-harvesting materials, but the complexity of the functional materials often impedes the ability to determine experimentally or theoretically how the properties of a molecule and the environment surrounding the molecule dictate light-harvesting efficiency.

We focus on the impact of these influences on charge transfer in the hexacyanoferrate(III) $[Fe(CN)_6^{3-}]$ coordination compound. The strong optical absorption and catalytic properties of coordination compounds make them a viable class of material for developing artificial photosynthetic complexes. In many of these complexes, the initial light absorption occurs in a component of the catalyst possessing high symmetry, such as a porphyrin or a polypyridyl unit.[12,18,19] The dynamics of the molecule and the surroundings prior to the separation of the electron and the hole will impact photocatalytic performance and influence the optimal design parameters for the catalyst. The electronic excited states of coordination complexes also provide an experimentally and theoretically tractable approach to investigating the dynamics of intramolecular energy migration and electron localization. We have investigated the dynamics of the electronic excited-state localization for the ligand-to-metal charge transfer (LMCT) excitation in $Fe(CN)_6^{3-}$ dissolved in acetonitrile (MeCN) and dimethyl sulfoxide (DMSO). In the electronic ground state, $Fe(CN)_6^{3-}$ has octahedral symmetry with six equivalent cyanide ligands. The LMCT excitation corresponds to a three-fold degenerate T_{1u}-symmetry excitation that does not instantaneously change the nuclear symmetry of the molecule.[20] While the spatial extent of the LMCT cannot be predicted *a priori*, the simplest analysis would predict the reduction of the iron atom from the ferric to the ferrous oxidation state and the oxidation of one cyanide ligand. The equivalence of the cyanide ligands, however, allows the electronic hole to hop from one ligand to another with a rate dictated by the strength of the electronic couplings between these ligands. Strong electronic coupling would lead to electron delocalization and the preservation of the octahedral symmetry found in the electronic ground state. Strong electronic coupling would also lead to the elimination of all anisotropy in the excited-state population, despite the linear polarization of the light used to generate the LMCT excited state. Alternatively, intramolecular distortion and solvation could stabilize the charge-transfer excited state, leading to electron localization and the reduction of the molecular symmetry. Should the rate of solvation and intramolecular distortion exceed the rate of electronic hopping between the ligands, optical excitation will

Received: August 3, 2011
Published: January 5, 2012

   dx.doi.org/10.1021/ja207306t | J. Am. Chem.Soc. 2012, 134, 2581−2588

lead to distinct cyanide ligands and an anisotropic population of charge-transfer excited states.

The importance of solvent- and intramolecular distortion-driven electron localization and electronic coupling-driven electron delocalization described above represent the key components to numerous theoretical studies of electronic structure and electron transfer in mixed-valence coordination chemistry, exemplified by the Creutz–Taube ion and donor–bridge–acceptor complexes.[21−30] As will be demonstrated, the electronic structure and dynamics of the electron hole on the cyanide ligands formed in the LMCT excited state of $Fe(CN)_6^{3-}$ represents a variant of the donor–bridge–acceptor structure, with the cyanide ligands functioning as donor and acceptor and the iron atom functioning as the bridge.

The interplay between electronic coupling and symmetry-breaking solvation and the impact of these counteracting forces on pump–probe anisotropy measurements have been investigated theoretically by Knox and Gulen, as well as Wynne and Hochstrasser, in molecules with high symmetry analogous to $Fe(CN)_6^{3-}$.[31−35] These theoretical investigations emphasize that degenerate excited states can influence the anisotropy in two distinct ways. When degenerate electronic states with orthogonal transition dipole moments couple strongly, electronic coupling induced electron hopping will lead to the complete loss of anisotropy. The theory also shows that probing of all degenerate excited states with transitions to a single final state generates pump–probe anisotropies in excess of the standard value of 0.4, as long as the generate excited states remain in a coherent superposition. For our measurements, this source of excess anisotropy does not apply because we also use a degenerate vibrational transition of T_{1u}-symmetry to probe the excited-state dynamics.

Despite multiple experimental anisotropy measurements, a predictive understanding of how electronic coupling, intramolecular distortion, and solvation influence the spatial extent of electronic excitations has not been achieved. The contradictory interpretations of anisotropy measurements for the metal-to-ligand charge transfer (MLCT) excited state of ruthenium(II) tris-bipyridine highlights this point. Wallin et al. conclude from their polarization resolved pump–probe measurements that the MLCT excited state of ruthenium tris-bipyridine delocalizes in less than 1 ps,[36] while Malone et al. concluded from their measurements that interligand hopping occurs with a 47 ps time constant.[37] In a third study performed by Yeh et al., they observed optical dephasing on the 100 fs time scale, but they did not report ultrafast interligand hopping of the MLCT excited state,[38] consistent with the measurements by Malone et al.[37]

We have used polarization-resolved UV pump–mid-IR probe spectroscopy[39−42] to study the electron localization dynamics of $Fe(CN)_6^{3-}$ dissolved in MeCN and DMSO. We have excited the LMCT excitation peaked at 420 nm with 400 nm pump pulses and probed the electronic excited-state dynamics with the CN stretch absorption band in the range from 2030 to 2120 cm^{-1} with the mid-IR polarization parallel and perpendicular to the UV pump polarization. Using the CN-stretch vibration to track the dynamics of electronic excited states presents three central advantages over the use of transient electronic absorption. (1) The transient signal does not have a stimulated emission component and the simplicity of the vibrational lineshapes allows us to clearly distinguish the excited-state absorption from the ground-state bleach (GSB) signal.[43] (2) For octahedral $Fe(CN)_6^{3-}$, only a three-fold degenerate T_{1u} CN-stretching mode leads to mid-IR absorption. Strong interligand electronic coupling in the LMCT excited state will lead to electron hole delocalization, preserve the octahedral symmetry, and lead to a single T_{1u} CN-stretch absorption band, while solvation and molecular distortion will lead to LMCT electron hole localization, a reduction in molecular symmetry to C_{4v}, and the splitting of the T_{1u} symmetry absorption into two bands, providing a clear spectroscopic signature of electron localization. (3) The CN-stretching modes have transition dipole moments lying parallel to the CN bonding axes of the molecule for both the ground and excited state, greatly simplifying the interpretation of the pump–probe anisotropy measurements compared to prior measurements using transient electronic spectroscopy where the direction of the excited-state absorption transition dipole moment can be difficult to determine either experimentally or theoretically.

EXPERIMENTAL SECTION

We purchased the potassium hexacyanoferrate(III) $[K_3Fe(CN)_6]$, tetraethylammonium chloride, MeCN, and DMSO from Sigma-Aldrich and used the materials as received. We prepared the $[(C_2H_5)_4N]_3Fe(CN)_6$ from $K_3Fe(CN)_6$ with an ion-exchange column to increase the solubility of $Fe(CN)_6^{3-}$ in DMSO and MeCN. We used a ~200 μm thick liquid flow cell with two CaF_2 windows for pump–probe measurements on a 40 mM $Fe(CN)_6^{3-}$ solution in DMSO or MeCN. The flow cell reduces the rate at which Prussian Blue builds up on the cell windows due to slow UV-induced dissociation of cyanide ligands. We prepared all samples with optical density around 1 at both 400 nm and 2100 cm^{-1}. UV–visible absorption spectra were measured on a Cary-50 Conc spectrometer. FTIR absorption spectra were measured on a Varian 1000 FT-IR spectrometer.

The pump and probe pulses were generated with a Ti:sapphire regenerative amplifier laser system (Spitfire, Spectra-Physics) with a 1 kHz repetition rate, 2.5 mJ pulse energy, 800 nm central wavelength, and a 50 fs full width at half-maximum (fwhm) pulse duration. The 400 nm pump pulse was produced by frequency-doubling one portion of the amplifier output with a 0.1 mm thick BBO crystal. We generated tunable mid-IR probe pulses by difference frequency mixing in $AgGaS_2$ the output of a near-IR optical parametric amplifier (OPA800CF, Spectra-Physics). These mid-IR pulses have a duration of roughly 70 fs fwhm with spectral width of about 200 cm^{-1}. The pump and probe beams were crossed in a liquid flow cell, with a probe diameter of 100 μm and a pump diameter of 400 μm. We used 2–5 μJ of 400 nm radiation for each pump pulse. We dispersed the transmitted probe beam with a grating spectrometer (iHR320, Horiba Jobin Yvon) onto a liquid nitrogen cooled 32 × 2 MCT pixel array detector (FPAS-6416-D, Infrared Systems Development Corp.) with a spectral resolution of 2 cm^{-1} per pixel.

COMPUTATIONAL METHOD

In addition to ultrafast spectroscopy measurements, we also used DFT calculations to investigate the electronic and nuclear structure of the $Fe(CN)_6^{3-}$ and $Ru(CN)_6^{3-}$ anions with the ADF[44,45] and Gaussian 09 software packages.[46] The details of these calculations can be found in the Supporting Information.

RESULTS

Figure 1 shows the UV–vis and mid-IR absorption spectra of $[(C_2H_5)_4N]_3Fe(CN)_6$ dissolved in MeCN and DMSO. Both solutions have an absorption peak at 420 nm which can be assigned to a LMCT ($^2T_{2g} \rightarrow {}^2T_{1u}$).[20,47] We excite the LMCT slightly off resonance at 400 nm. The vibrational absorption band in the electronic ground state at around 2100 cm^{-1} corresponds to the T_{1u} triply degenerate CN-stretching mode.[48−50]

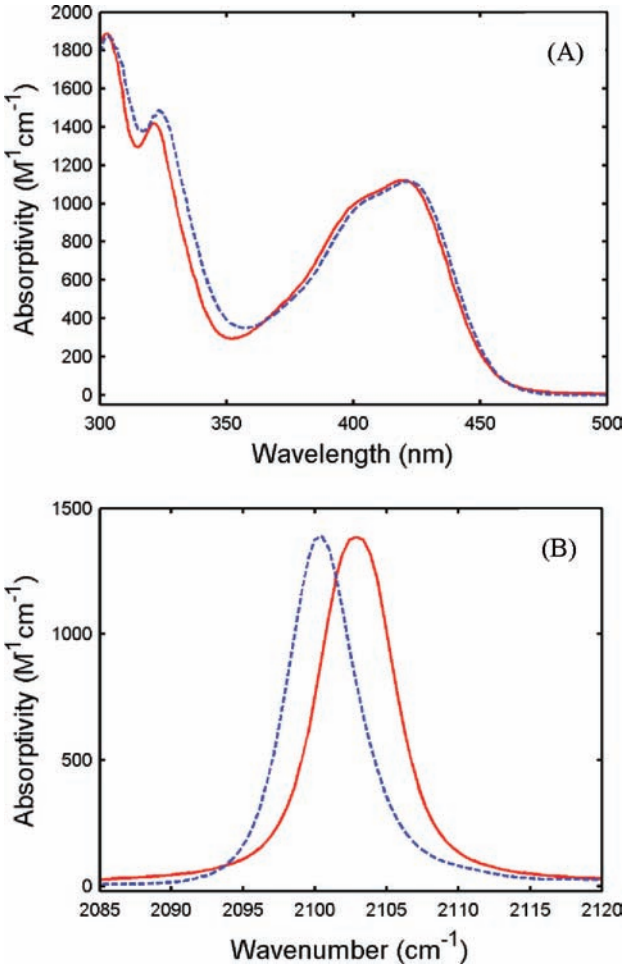

Figure 1. (A) UV–vis and (B) mid-IR absorption spectra of $Fe(CN)_6^{3-}$ in MeCN (red traces) and DMSO (blue traces).

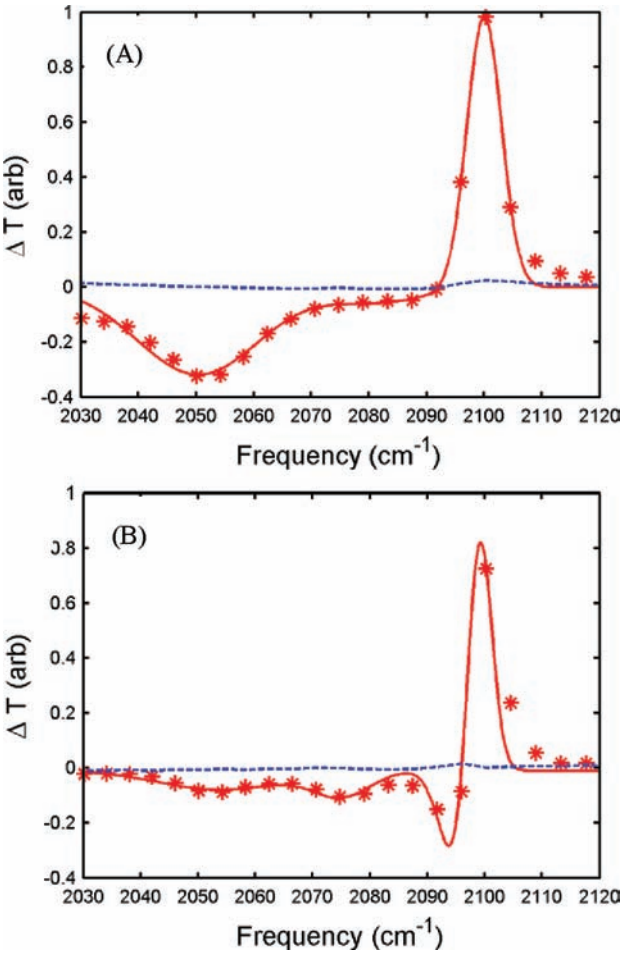

Figure 2. Isotropic (red points) and $S_{\parallel} - S_{\perp}$ difference (blue traces) transient spectra for $Fe(CN)_6^{3-}$ in DMSO at (A) 0.2 and (B) 5 ps time delay. The solid red line is the fitting of isotropic transient spectra.

We measured the transient absorption dynamics in the CN-stretch region of the mid-IR absorption spectrum induced by 400 nm excitation with the mid-IR probe pulse polarization parallel and perpendicular to the pump pulse polarization.[39,41,43,51,52] We have measured the time and frequency dependence of the isotropic signal, $S_{iso}(t) = S_{\parallel}(t) + 2S_{\perp}(t)$, the difference signal, $S_{diff}(t) = S_{\parallel}(t) - S_{\perp}(t)$, and the anisotropic signal, $r(t)$,

$$r(t) = \frac{S_{\parallel}(t) - S_{\perp}(t)}{S_{iso}(t)} \quad (1)$$

where $S_{\parallel}$ represents the signal with parallel linear polarizations for the pump and probe pulses, and $S_{\perp}$ represents the signal with perpendicular linear polarizations for the pump and probe pulses. The S_{iso} and S_{diff} spectra for a 0.2 ps time delay, in Figure 2A for the DMSO solution and Figure 3A for the MeCN solution, show a single GSB with a positive change in transmitted intensity and a single excited-state absorption band with a negative change in transmitted intensity. Neither the GSB nor the excited-state absorption exhibits a measurable S_{diff}. For the GSB, the lack of anisotropy reflects the isotropic absorption of the T_{1u}-symmetry CN stretch. The same argument cannot be used to explain the lack of anisotropy for the excited-state absorption plotted in Figure 4 because the linear polarization of the pump pulse will initially produce an anisotropic distribution of excited states. As will be discussed shortly, the isotropic, single excited-state absorption provides strong experimental evidence for strong electronic coupling between ligands and electron hole delocalization on all six cyanide ligands.

The single excited-state absorption band decay leads to the formation of two excited-state absorption bands, as can be seen in transient absorption spectra measured for a 5 ps time delay, shown in Figures 2B and 3B. The time-dependent population dynamics for the GSB and the two distinct excited states can also be found in Figure 5. As can be seen in Figure 6A,C, both rise times for the two new excited-state absorption bands correlate with the decay of the initial excited-state absorption, strongly indicating that both new peaks result from a single excited-state species. The transition from a single excited-state CN-stretch absorption band to two excited-state CN-stretch absorption bands provides strong evidence for a reduction in molecular symmetry.

This change in symmetry could result from either excited-state electron localization or relaxation from the LMCT excited state to the $^4T_1$ ligand field excited state of $Fe(CN)_6^{3-}$. Electron localization will reduce the symmetry of the molecule, but quartet state formation will also reduce the symmetry because the quartet state will have a single electron in the E_g level, leading to Jahn–Teller distortion. Quantum chemical calculations also predict a D_{4h} symmetry for the $^4T_1$ ligand field

dx.doi.org/10.1021/ja207306t | J. Am. Chem.Soc. 2012, 134, 2581–2588

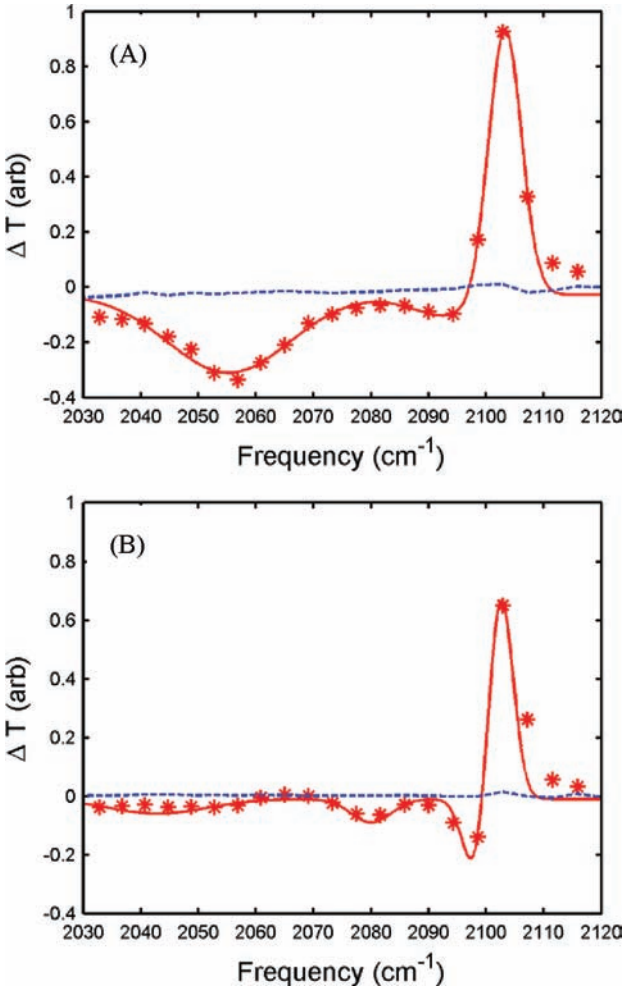

Figure 3. Isotropic (red points) and $S_{\parallel} - S_{\perp}$ difference (blue traces) transient spectra for $Fe(CN)_6^{3-}$ in MeCN at (A) 0.2 and (B) 5 ps time delay. The solid red line is the fitting of isotropic transient spectra.

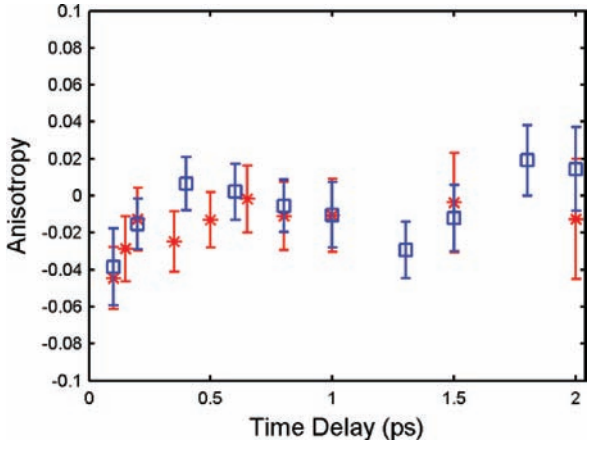

Figure 4. Time-dependent anisotropy for the initially generated LMCT excited-state absorption of $Fe(CN)_6^{3-}$ measured at 2055 cm^{-1} for MeCN (red points) and 2050 cm^{-1} for DMSO (blue points). Error bars are included for each data point.

excited state with two mid-IR-active CN-stretch vibrational transition frequencies. To differentiate between electron hole localization and ligand field excitation, we have also studied the dynamics of $Ru(CN)_6^{3-}$ initiated by LMCT excitation.

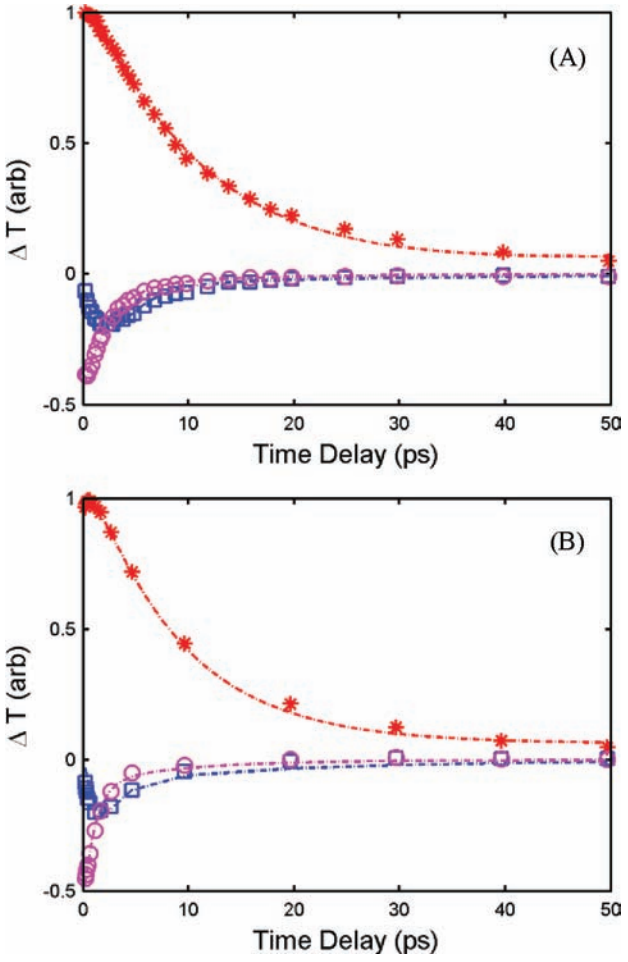

Figure 5. Plot of the time-dependent change in transmission for the isotropic pump–probe signal. (A) Population dynamics for the GSB measured at 2100 cm^{-1} (red points), the initially generated delocalized LMCT excited-state absorption band measured at 2054 cm^{-1} (purple points), and the localized LMCT excited-state absorption band measured at 2091 cm^{-1} (blue points) of $Fe(CN)_6^{3-}$ measured in DMSO. (B) Population dynamics measured at 2102 (red), 2056 (purple), and 2094 cm^{-1} (blue) in MeCN. The lines show the kinetic model fits of experimental data.

$Ru(CN)_6^{3-}$ has a larger ligand field splitting, which precludes relaxation from the LMCT to any ligand field excited states. This conclusion has been supported by quantum chemical calculations. The lowest-energy ligand field excited state has a calculated excitation energy of ~1 eV for $Fe(CN)_6^{3-}$ and ~3 eV for $Ru(CN)_6^{3-}$. For $Ru(CN)_6^{3-}$, this energy exceeds the expremental LMCT excitation energy of 2.67 eV,[53] but not the LMCT excitation energy of 2.91 eV for $Fe(CN)_6^{3-}$.[20] Given that hybrid functional DFT calculations tend to over stabilize electronic states with higher spin multiplicity, these calculated energy differences should be viewed as lower bounds for the energy difference between the lowest energy doublet and quartet states.[54,55] A more detailed discussion of the theoretical calculations can be found in the Supporting Information. This conclusion has also been drawn previously from photoluminescence measurements.[53,56]

Even though ligand field excited states do not provide an energetically accessible relaxation channel for $Ru(CN)_6^{3-}$, we still observe qualitatively equivalent dynamics for the ruthenium and iron compounds, as shown in the Supporting Information.

dx.doi.org/10.1021/ja207306t | J. Am. Chem.Soc. 2012, 134, 2581–2588

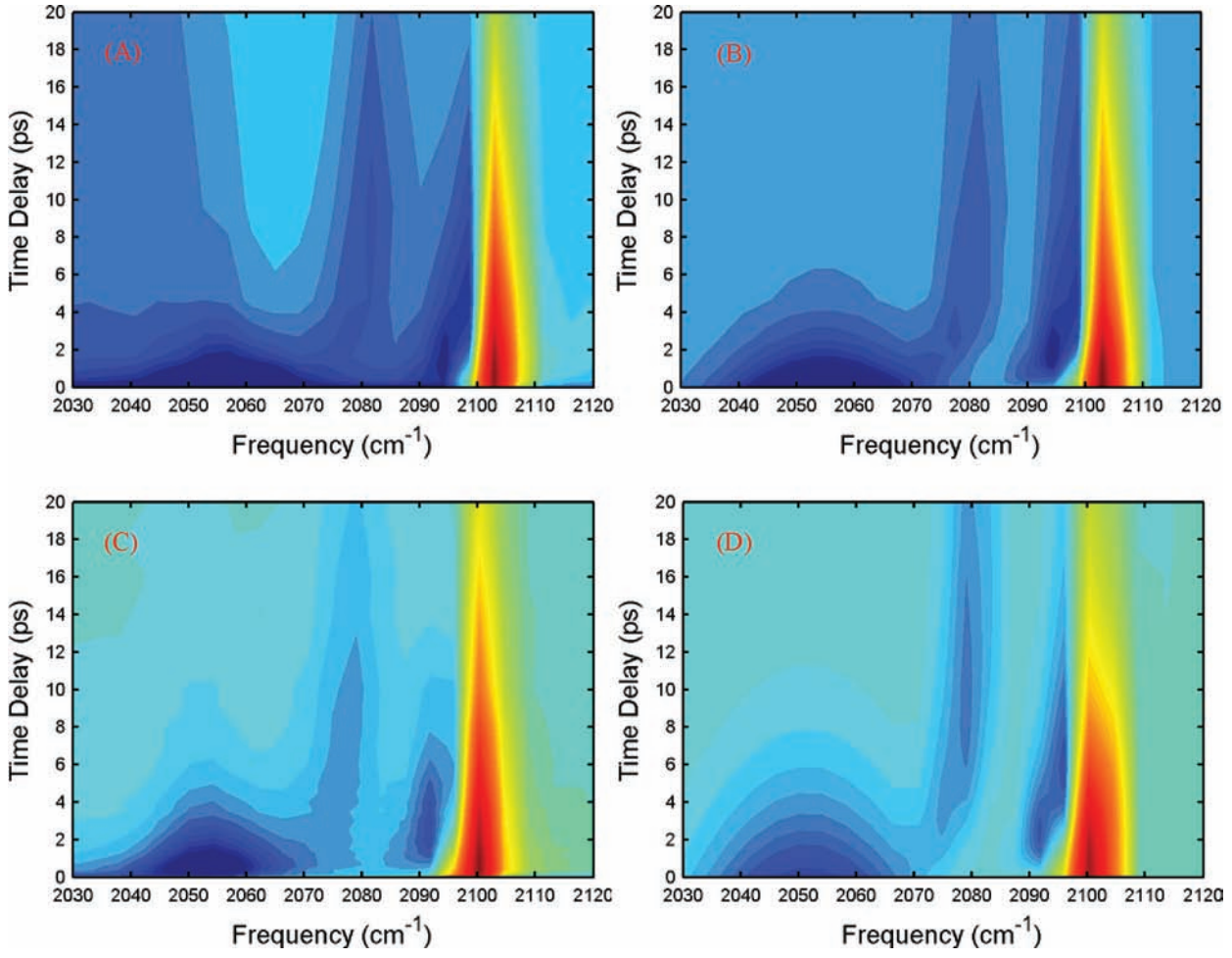

Figure 6. (Left) Two-dimensional UV pump−mid-IR probe isotropic transient spectra as a function of probe delay time and frequency for $Fe(CN)_6^{3-}$ in (A) MeCN and (C) DMSO. (Right) Global fitting to the kinetic model described in the text is shown in (B) for the MeCN solutions and (D) for the DMSO solution.

For this reason, we have concluded that the reduction in excited-state symmetry associated with the transition from the initial electronic excited state to the secondary excited state results from electron hole localization.

We have modeled the population dynamics measured experimentally with a sequential three-state, two-steps kinetic model,

$$D_{CT} \xrightarrow{k_1} L_{CT} \xrightarrow{k_2} H_G$$

where D_{CT} corresponds to the delocalized LMCT excited state, L_{CT} the localized LMCT excited state, H_G the depletion of the electronic ground-state population, k_1 the rate of decay from D_{CT} to L_{CT}, and k_2 the rate of L_{CT} decay back to the electronic ground state. The kinetic equations for the time-dependent population dynamics of these three species can be found in the Supporting Information.

We have used these kinetic equations, along with Gaussian lineshapes for the peaks in the vibrational spectrum, to fit the full two-dimensional data sets shown in Figure 6A,C. The best fits can be found in Figure 6B,D and the rate constants and excited-state CN-stretch frequencies in Table 1. The comparison between the experimental data and the best fit can also be found in Figures 2, 3, 5, and 6.

The two CN-stretch vibrations of the localized LMCT excited state also have time-dependent frequencies, while the initially excited delocalized excited state has a time independent frequency. This additional dynamical aspect of the experimental results can be seen clearly in Figure 6A,C. The fit to the experimental data gives time constants for the shifts equivalent to the time constant for the formation of the localized LMCT state, k_1^{-1}, for both MeCN and DMSO. The origin of these spectral dynamics will be discussed in the following section.

Table 1. CN-Stretch Vibrational Frequencies (cm^{-1}) and Time Constants (ps) Based on the Global Fitting of MeCN and DMSO Solution Results

	ω-D_{CT}	ω-L_{CT}	ω-L_{CT}	ω-H_G	k_1^{-1}	k_2^{-1}
DMSO	2050	2079	2099	2100	4.9	28.1
MeCN	2055	2081	2101	2104	1.9	17.5

DISCUSSION

The three-fold degeneracy of the LMCT electronic state of $Fe(CN)_6^{3-}$ excited in our experiment allows facile excited-state population transfer between the three-fold degenerate states. In the theory of Wynne and Hochstrasser,[31,32] excited-state hopping will occur with a rate Γ, lead to equal excited-state populations in the three LMCT excited states, and eliminate all excited-state anisotropy, since these states have optically orthogonal transition dipole moments. Ignoring the influence of molecular rotation and optical dephasing, Wynne and

dx.doi.org/10.1021/ja207306t | J. Am. Chem.Soc. 2012, 134, 2581−2588

Hochstrasser predict a time-dependent anisotropy given by, $r(t) = {}^{2}/_{5}\exp(-3\Gamma t)$. Strong electronic coupling between the degenerate excited states will lead to an isotropic population of excited states, as seen in our experiments at the earliest time. The roughly 200 fs temporal resolution of our experiment, as dictated by the time required to distinguish the excited-state absorption at roughly 2050 cm^{-1} from the ground-state absorption at roughly 2100 cm^{-1}, sets a lower bound on the electron hopping rate $3\Gamma \geq 5\ ps^{-1}$, since we do not observe any excited-state anisotropy in the transient spectra measured for a pump−probe time delay of 200 fs. This can be most clearly seen in Figure 4.

The single CN-stretch excited-state absorption band initially generated by electronic excitation provides further evidence for electron hole delocalization on all six cyanide ligands. While the optical excitation initially leads to the formation of a delocalized LMCT excited state, we see the relaxation of this initial excited state to a second electronic excited state with two distinct CN-stretch absorption bands, as clearly seen in Figures 2, 3, 5, and 6. These peaks associated with the CN-stretch transitions of L_{CT} have the same rise times, which also match the decay time of the initial electronic excited state. This observation leads us to conclude that the initial excited-state decay forms only one secondary electronic excited state, despite the presence of two CN-stretch absorption bands.

Since both CN-stretch vibrational transitions result from a single excited-state species, the symmetry of $Fe(CN)_6^{3-}$ must be reduced upon the relaxation from the first electronic excited state to this secondary excited state. We attribute the reduction in symmetry to the localization of the LMCT to a single cyanide ligand, a localization driven by solvent and solute reorganization. We have two primary reasons for attributing the observed relaxation to LMCT excited-state localization. First, the highly similar dynamics for $Fe(CN)_6^{3-}$ and $Ru(CN)_6^{3-}$ indicates the same dynamical process occurs for both complexes, making electronic relaxation to a ligand field excited state highly unlikely, since the LMCT excited state is the lowest energy electronic excited state of $Ru(CN)_6^{3-}$. Additionally, the rate of electron localization and the time-dependent shift of the CN-stretch frequencies for the electron localized excited state show a strong solvent dependence. The solvent dependence of the localization rate and localized state spectral shift (that is solvation of the localized state) matches the expectation that LMCT localization would require significant solvent reorganization. While the solvent-dependent localization rate could also result from a solvent-dependent barrier height for solute reorganization, this cannot explain why the frequency shift of the localized state CN-stretching bands and the electron localization occur with the same time constant.

The initial delocalization of the LMCT excited state in our measurements resembles the measurements and interpretation of Wallin et al. in ruthenium tris-bipyridine and Wynne and Hochstrasser for metal porphyrin complexes,[34−36] though the appearance of electron localization on the picosecond time scale has not been reported in these prior studies. The observation of time-dependent excited-state localization, however, resembles the findings of Yeh et al. for ruthenium tris-bipyridine.[38] They observed an ultrafast decay of the anisotropy to a value of 0.4, which they attributed to dephasing dynamics caused by the inertial rotational dynamics of the solvent. This anisotropy then persisted for multiple picoseconds, indicative of the localization of the excited-state electron on a single bipyridine ligand. They report no evidence for sub-picosecond electronic hopping between ligands in their measurements. In our measurements, the inertial solvation does not provide sufficient driving force for excited-state localization. The localization requires a slower relaxation involving yet-to-be-determined solute and solvent degrees of freedom. Interestingly, the localization time constants appear measurably slower than the canonical solvation relaxation time constants observed with time-resolved fluorescence Stokes shift measurements and photon echo spectroscopy.[57−61] Maroncelli and co-workers have measured the mean solvation time constant of MeCN to be 0.26 ps, and 2.0 ps for DMSO.[61] While the rate of electron localization measured by Yeh et al. in MeCN resembles the rate of coumarin excited-state solvation measured by Maroncelli and co-workers, our results indicate that the solvation mechanism for excited-state electron localization of the LMCT state of $Fe(CN)_6^{3-}$ in MeCN proceeds with a time constant of 1.9 ps, and 4.9 ps in DMSO. This significant variance in time constant could be indicative of solvation dynamics distinct from those measured for coumarin 153. As emphasized by the simulation studies of Schwartz and co-workers,[62] inertial dynamics dominate when the solvation does not require significant center of mass motion for the solvent molecules. Given that the solvation and localization of the LMCT state requires changes in metal−ligand bond lengths, this solvation process may require significant translational motion of solvent molecules. Alternatively, the intramolecular reorganization of the metal−ligand bonding with a solvent-dependent barrier could also be the source of these picosecond dynamics.

■ CLOSING REMARKS

The ligand-to-metal charge-transfer excited state of hexacyanoferrate(III) provides a simple molecular system for investigating the influence of interligand electronic coupling, intramolecular distortion, and excited-state solvation on the electronic structure of charge-transfer excited states. Solvent- and intramolecular distortion-driven electron localization and electronic coupling-driven electron delocalization represent the key components to numerous theoretical descriptions of electronic structure and electron transfer in mixed-valence coordination chemistry and donor−bridge−acceptor complexes.

Our ultrafast UV pump−mid-IR probe measurements have clearly shown that the LMCT excited state of $Fe(CN)_6^{3-}$ can be viewed as a model system for studying the dynamics of electron localization in a donor−bridge−acceptor structure, with the cyanide ligands functioning as donor and acceptor and the iron atom functioning as the bridge. The measurements have clearly shown that electron localization requires structural reorganization on the picosecond time scale with a rate that depends significantly on the solvent. The electron localization proceeds more slowly than generally expected for dipolar solvation dynamics in acetonitrile and dimethyl sulfoxide. This could indicate that the inertial rotational dynamics that generally dominate solvation dynamics in polar solvents do not dominate the dynamics of electron localization for $Fe(CN)_6^{3-}$ or a solvent-controlled barrier height associated with intramolecular distortion. Addressing this question will require theoretical studies of the excited-state dynamics in the presence of solvent, but the relative simplicity of $Fe(CN)_6^{3-}$ makes such calculations feasible.

■ ASSOCIATED CONTENT

Supporting Information

Ligand field excited-state energies calculated with 10Dq and Racah parameters; ligand field excited-state energies determined with quantum chemistry calculations; dynamics of solvent-mediated electron localization in electronically excited hexacyanoruthenate; kinetic modeling of the experimental population dynamics; theoretically calculated geometries for hexacyanoferrate and hexacyanoruthenate; complete ref 46. This material is available free of charge via the Internet at http://pubs.acs.org.

■ AUTHOR INFORMATION

Corresponding Author

kgaffney@slac.stanford.edu

Present Address

[§]Department of Chemistry and Chemical Biology, Harvard University, Cambridge, MA 02138

■ ACKNOWLEDGMENTS

We thank Dr. Patrick Frank for helpful discussions concerning synthesis of the hexacyanoruthenate complexes. This research is supported through the PULSE Institute at SLAC National Accelerator Laboratory by the U.S. Department of Energy, Office of Basic Energy Sciences.

■ REFERENCES

(1) van Grondelle, R.; Dekker, J. P.; Gillbro, T.; Sundstrom, V. *Biochim. Biophys. Acta* **1994**, *1187*, 1−65.
(2) Scholes, G. D.; Fleming, G. R. *J. Phys. Chem. B* **2000**, *104*, 1854−1868.
(3) Cho, M. H.; Vaswani, H. M.; Brixner, T.; Stenger, J.; Fleming, G. R. *J. Phys. Chem. B* **2005**, *109*, 10542−10556.
(4) van Grondelle, R.; Novoderezhkin, V. I. *Phys. Chem. Chem. Phys.* **2006**, *8*, 793−807.
(5) Read, E. L.; Engel, G. S.; Calhoun, T. R.; Mancal, T.; Ahn, T. K.; Blankenship, R. E.; Fleming, G. R. *Proc. Natl. Acad. Sci. U.S.A.* **2007**, *104*, 14203−14208.
(6) Collini, E.; Wong, C. Y.; Wilk, K. E.; Curmi, P. M. G.; Brumer, P.; Scholes, G. D. *Nature* **2010**, *463*, 644−U69.
(7) Fidder, H.; Terpstra, J.; Wiersma, D. A. *J. Chem. Phys.* **1991**, *94*, 6895−6907.
(8) Potma, E. O.; Wiersma, D. A. *J. Chem. Phys.* **1998**, *108*, 4894−4903.
(9) Thompson, A. L.; Gaab, K. M.; Xu, J. J.; Bardeen, C. J.; Martinez, T. J. *J. Phys. Chem. A* **2004**, *108*, 671−682.
(10) Collini, E.; Scholes, G. D. *Science* **2009**, *323*, 369−373.
(11) Spano, F. C. *Acc. Chem. Res.* **2010**, *43*, 429−439.
(12) Wasielewski, M. R. *J. Org. Chem.* **2006**, *71*, 5051−5066.
(13) Nocera, D. G. *Acc. Chem. Res.* **1995**, *28*, 209−217.
(14) Holstein, T. *Ann. Phys.* **1959**, *8*, 343−389.
(15) Holstein, T. *Ann. Phys.* **1959**, *8*, 325−342.
(16) Ge, N. H.; Wong, C. M.; Lingle, R. L.; McNeill, J. D.; Gaffney, K. J.; Harris, C. B. *Science* **1998**, *279*, 202−205.
(17) Miller, A. D.; Bezel, I.; Gaffney, K. J.; Garrett-Roe, S.; Liu, S. H.; Szymanski, P.; Harris, C. B. *Science* **2002**, *297*, 1163−1166.
(18) Gust, D.; Moore, T. A.; Moore, A. L. *Acc. Chem. Res.* **2001**, *34*, 40−48.
(19) Sun, L. C.; Hammarstrom, L.; Akermark, B.; Styring, S. *Chem. Soc. Rev.* **2001**, *30*, 36−49.
(20) Alexander, J. J.; Gray, H. B. *J. Am. Chem. Soc.* **1968**, *90*, 4260−4271.
(21) Brunschwig, B. S.; Creutz, C.; Sutin, N. *Chem. Soc. Rev.* **2002**, *31*, 168−184.
(22) Demadis, K. D.; Hartshorn, C. M.; Meyer, T. J. *Chem. Rev.* **2001**, *101*, 2655−2685.
(23) Kaim, W.; Klein, A.; Glockle, M. *Acc. Chem. Res.* **2000**, *33*, 755−763.
(24) Lambert, C.; Noll, G.; Schelter, J. *Nat. Mater.* **2002**, *1*, 69−73.
(25) Londergan, C. H.; Salsman, J. C.; Ronco, S.; Dolkas, L. M.; Kubiak, C. P. *J. Am. Chem. Soc.* **2002**, *124*, 6236−6237.
(26) Barbara, P.; Meyer, T.; Ratner, M. *J. Phys. Chem.* **1996**, *100*, 13148−13168.
(27) Walker, G. C.; Barbara, P. F.; Doorn, S. K.; Dong, Y. H.; Hupp, J. T. *J. Phys. Chem.* **1991**, *95*, 5712−5715.
(28) Wang, C. F.; Mohney, B. K.; Akhremitchev, B. B.; Walker, G. C. *J. Phys. Chem. A* **2000**, *104*, 4314−4320.
(29) Son, D. H.; Kambhampati, P.; Kee, T. W.; Barbara, P. F. *J. Phys. Chem. A* **2002**, *106*, 4591−4597.
(30) Kambhampati, P.; Son, D. H.; Kee, T. W.; Barbara, P. F. *J. Phys. Chem. A* **2000**, *104*, 10637−10644.
(31) Wynne, K.; Hochstrasser, R. M. *Chem. Phys.* **1993**, *171*, 179−188.
(32) Wynne, K.; Hochstrasser, R. M. *J. Raman Spectrosc.* **1995**, *26*, 561−569.
(33) Knox, R. S.; Gulen, D. *Photochem. Photobiol.* **1993**, *57*, 40−43.
(34) Galli, C.; Wynne, K.; Lecours, S. M.; Therien, M. J.; Hochstrasser, R. M. *Chem. Phys. Lett.* **1993**, *206*, 493−499.
(35) Wynne, K.; Lecours, S. M.; Galli, C.; Therien, M. J.; Hochstrasser, R. M. *J. Am. Chem. Soc.* **1995**, *117*, 3749−3753.
(36) Wallin, S.; Davidsson, J.; Modin, J.; Hammarstrom, L. *J. Phys. Chem. A* **2005**, *109*, 4697−4704.
(37) Malone, R. A.; Kelley, D. F. *J. Chem. Phys.* **1991**, *95*, 8970−8976.
(38) Yeh, A. T.; Shank, C. V.; McCusker, J. K. *Science* **2000**, *289*, 935−938.
(39) Moore, J. N.; Hansen, P. A.; Hochstrasser, R. M. *Proc. Natl. Acad. Sci. U.S.A.* **1988**, *85*, 5062−5066.
(40) Lim, M.; Jackson, T. A.; Anfinrud, P. A. *Science* **1995**, *269*, 962−966.
(41) Lim, M. H.; Jackson, T. A.; Anfinrud, P. A. *Nat. Struct. Biol.* **1997**, *4*, 209−214.
(42) Jha, S. K.; Ji, M. B. A.; Gaffney, K. J.; Boxer, S. G. *Proc. Natl. Acad. Sci. U.S.A.* **2011**, *108*, 16612−16617.
(43) Usman, A.; Mohammed, O. F.; Nibbering, E. T. J.; Dong, J.; Solntsev, K. M.; Tolbert, L. M. *J. Am. Chem. Soc.* **2005**, *127*, 11214−11215.
(44) Guerra, C. F.; Snijders, J. G.; te Velde, G.; Baerends, E. J. *Theor. Chem. Acc.* **1998**, *99*, 391−403.
(45) Velde, G. T.; Bickelhaupt, F. M.; Baerends, E. J.; Guerra, C. F.; Van Gisbergen, S. J. A.; Snijders, J. G.; Ziegler, T. *J. Comput. Chem.* **2001**, *22*, 931−967.
(46) Frisch, M. J.; et al. *Gaussian 09*, Revision B.01; Gaussian, Inc.: Wallingford, CT, 2010.
(47) Naiman, C. S. *J. Chem. Phys.* **1961**, *35*, 323−328.
(48) Sando, G. M.; Zhong, Q.; Owrutsky, J. C. *J. Chem. Phys.* **2004**, *121*, 2158−2168.
(49) Ohta, K.; Maekawa, H.; Tominaga, K. *J. Phys. Chem. A* **2004**, *108*, 1333−1341.
(50) Kettle, S. F. A.; Aschero, G. L.; Diana, E.; Rossetti, R.; Stanghellini, P. L. *Inorg. Chem.* **2006**, *45*, 4928−4937.
(51) Ansari, A.; Szabo, A. *Biophys. J .* **1993**, *64*, 838−851.
(52) Heyne, K.; Mohammed, O. F.; Usman, A.; Dreyer, J.; Nibbering, E. T. J.; Cusanovich, M. A. *J. Am. Chem. Soc.* **2005**, *127*, 18100−18106.
(53) Vogler, A.; Kunkely, H. *Inorg. Chim. Acta* **1981**, *53*, L215−L216.
(54) Paulsen, H.; Duelund, L.; Winkler, H.; Toftlund, H.; Trautwein, H. X. *Inorg. Chem.* **2001**, *40*, 2201−2203.
(55) Daku, L. M. L.; Vargas, A.; Hauser, A.; Fouqueau, A.; Casida, M. E. *Chemphyschem* **2005**, *6*, 1393−1410.
(56) Vogler, A.; Kunkely, H. *Top. Curr. Chem.* **2001**, *213*, 143−182.
(57) de Boeij, W. P.; Pshenichnikov, M. S.; Wiersma, D. A. *Annu. Rev. Phys. Chem.* **1998**, *49*, 99−123.
(58) Stratt, R. M.; Maroncelli, M. *J. Phys. Chem.* **1996**, *100*, 12981−12996.

(59) Joo, T. H.; Jia, Y. W.; Yu, J. Y.; Lang, M. J.; Fleming, G. R. *J. Chem. Phys.* **1996**, *104*, 6089−6108.
(60) Fleming, G. R.; Cho, M. H. *Annu. Rev. Phys. Chem.* **1996**, *47*, 109−134.
(61) Horng, M. L.; Gardecki, J. A.; Papazyan, A.; Maroncelli, M. *J. Phys. Chem.* **1995**, *99*, 17311−17337.
(62) Aherne, D.; Tran, V.; Schwartz, B. *J. Phys. Chem. B* **2000**, *104*, 5382−5394.